Journal Name

ARTICLE TYPE

Cite this: DOI: 10.1039/xxxxxxxxxx

Validating an optimized GAFF force field for liquid crystals: T_{NI} predictions for bent-core mesogens and the first atomistic predictions of a dark conglomerate phase†

Nicola Jane Boyd [a] and Mark R. Wilson*[a]

Received Date
Accepted Date

DOI: 10.1039/xxxxxxxxxx

www.rsc.org/journalname

The GAFF-LCFF force field [N. J. Boyd *et al.*, Phys. Chem. Chem. Phys., 2015, 17, 24851] is tested and further improved for use in the simulation of bent-core liquid crystal mesogens. Atomistic simulations are carried out on four systems of bent-core nematogens based on a central *bis*-(phenyl)oxadiazole (ODBP) motif, providing excellent agreement with experimental, T_{NI}, transition temperatures. Simulations of one bent-core system (C5-Ph-ODBP-Ph-OC12) indicate the presence of a dark conglomerate (DC) phase, with the prediction of a highly unusual nematic to DC phase transition.

Introduction

In order to fully exploit the design process of liquid crystals, a robust understanding of the relationship between molecular structure and the properties of liquid-crystalline mesophases is vital. In particular, the phase transition temperatures of many mesophases are very sensitive to minor changes in molecular structure. For example, the variation in number of aliphatic carbon atoms in the 4-alkyl-4'-*n*-cyanobiphenyl series (*n*CB) not only results in the alternation of clearing temperatures (the odd-even effect) but also determines the range of nematic and smectic phases.[1,2] The addition of a single lateral methyl group to the aromatic core of a bent-core mesogen, based on the *bis*-(phenyl)oxadiazole motif, results in a huge reduction in the T_{NI} compared with the non-methylated derivative.[3] In another bent-core system, simply replacing the alkyl chains attached to the bent-core unit with alkoxy chains introduces a B4 banana phase, displaying a chiral superstructure, which is absent for the alkyl chain counterpart (compounds 1b and 48a in reference[4]). This remarkable sensitivity to molecular detail arises from a complex interplay between energetic effects (the molecular interactions through electrostatic, dispersive and inductive forces) and entropic ones (positional, orientational and conformational distributions).[5]

Molecular dynamic (MD) simulations based on atomistic force fields are particularly suitable for investigative studies of liquid crystal (LC) systems. They have the potential to accurately predict the macroscopic properties of a given substance in its condensed phase regardless of the availability of experimental data, identify structure-property relationships, and provide a detailed perspective of the molecular organization in LC phases.[2,6] In addition, an atomistic level of description can provide a useful complement to experimental studies, such as aiding in the interpretation of results obtained from X-ray diffraction and nuclear magnetic (NMR) experiments. The quality of results from atomistic MD simulations, however, is strongly dependent on the potential functions and parameters employed in the force field, and hence its description of the molecular geometry and intermolecular interactions.[7]

Two of the most sensitive liquid crystal macroscopic properties to reproduce, and crucial for technological applications, are the T_{NI} transition temperature (clearing temperature) and the thermal stability range of the nematic phase.[8] Unfortunately, the use of standard force fields for the study of liquid crystal systems often produces poor results. For example, simulated results for 5CB and 8CB employing AMBER, OPLS and the General AMBER force field (GAFF) have reported transition temperatures (T_{NI} and T_{SN}) approximately 33 - 120 K above experimental values.[2,9,10] A recent study employing GAFF resulted in a simulated $T_{NI} \approx 60$ K greater than the experimental value for the nematogen 1,3-benzenedicarboxylic acid,1,3-*bis*(4-butylphenyl)ester.[11]

One route to obtaining an accurate force field for the investigation of LC materials is to parametrize the force field entirely from *ab initio*, electronic structure calculations.[5,8,12–18] The main advantage of this method is that it is possible to account for all the

[a] *Department of Chemistry, Durham University, South Road, Durham, DH1 3LE, United Kingdom.*
* *Author for correspondence. E-mail: mark.wilson@durham.ac.uk*
† Electronic Supplementary Information (ESI) available: force field parameters and chemical structures of fragment molecules studied. See DOI: 10.1039/b000000x/

relevant physics of intermolecular interactions within the context of the force field, and this can be systematically improved by increasing the level of theory.[19] In addition, a wide range of structural and dynamical properties can be described which do not rely on any experimental data.[5]

Alternatively the description of LC systems can be improved through revision of the original parameters of existing empirically derived force fields. This approach has led to significant improvements in the predicted thermodynamic, structural and dynamic properties of LC systems.[2,7,20–25]

In a recent study by the current authors, the GAFF force field was optimized in order to obtain a force field suitable for a range of liquid crystals. The amended force field, GAFF-LCFF, was initially tested on a typical calamitic nematogen, 1,3-benzenedicarboxylic acid,1,3-*bis*(4-butylphenyl)ester, and successfully predicted a T_{NI} temperature within 5 K of the experimental value, reducing the original GAFF predicted temperature by almost 60 K.[11] It was proposed that a combination of factors were responsible for the overestimation of T_{NI} by GAFF (and related force fields), predominantly alkyl chains which are too stiff, ester groups which are not flexible enough and LJ interactions which are slightly too attractive. Each factor is addressed in GAFF-LCFF. Very recently, GAFF-LCFF has also been reported to significantly improve the simulated order parameters for the cyanobiphenyl-based nematic host mixture, E7.[26]

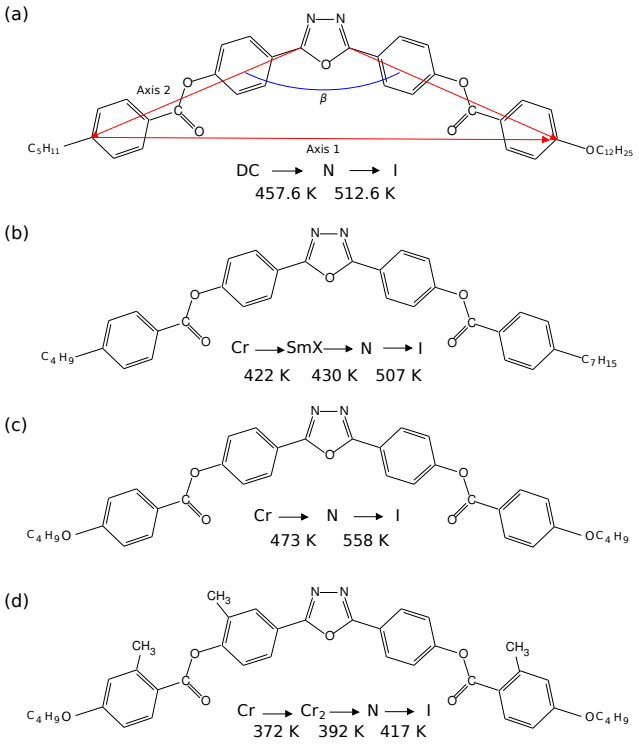

Fig. 1 The chemical structures and phase transitions of the bent-core mesogens. a) C5-Ph-ODBP-Ph-OC12 b) C4-Ph-ODBP-Ph-C7 c) C4O-Ph-ODBP and d) C4O-Ph-ODBP(trimethylated)

In this paper, our objectives are to test, and further improve GAFF-LCFF, by making phase behaviour predictions for a series of challenging materials based on a bent-core *bis*-(phenyl)oxadiazole (ODBP) motif; systems for which many unusual properties have been experimentally observed.[3,27–34] (see Fig.1 for chemical structures and abbreviated names).

Preliminary tests on four ODBP bent-core mesogens, employing the original GAFF force field resulted in T_{NI} temperatures in the range of 60 K to 110 K higher than the experimental values. The results presented in this paper show that with the incorporation of some further minor parameter refinements, to account for the chemical details specific to these four bent-core systems, GAFF-LCFF provides T_{NI} estimates within 10 K of experimental values. In addition, the atomistic simulations show a second phase transition into the experimentally observed dark conglomerate (DC) phase for the C5-Ph-ODBP-Ph-OC12 system. As far as the authors are aware, this is the first example of a fully atomistic simulation indicating the presence of a DC phase.

Computational Methods

Simulation Details

All calculations were performed using the GROMACS 4.5.5 package[35] using a modified version of the GAFF force field (as described in detail below). The energy function employed in the MD simulations is given by

$$
\begin{aligned}
E^{\mathrm{MM}} &= \sum_{\text{bonds}} K_{\mathrm{r}}(r-r_{\mathrm{eq}})^2 + \sum_{\text{angles}} K_\theta(\theta-\theta_{\mathrm{eq}})^2 \qquad (1)\\
&+ \sum_{\mathrm{n}=0}^{5} C_n(\cos(\psi))^n + \sum_{\text{impropers}} k_d\,(1+\cos(n_d\omega-\omega_d))\\
&+ \sum_{i>j}^{N}\left[\left(4\varepsilon_{ij}\left(\frac{\sigma_{ij}}{r_{ij}}\right)^{12}-\left(\frac{\sigma_{ij}}{r_{ij}}\right)^{6}\right)+\frac{1}{4\pi\varepsilon_0}\frac{q_iq_j}{r_{ij}}\right],
\end{aligned}
$$

where r_{eq}, θ_{eq} are respectively natural bond lengths and angles, K_r, K_θ and C_n are respectively bond, angle, and torsional force constants, σ_{ij} and ε_{ij} are the usual Lennard-Jones parameters and q_i, q_j are partial electronic charges. Changes in E^{MM} arising from deviations in improper dihedral angles, ω, are represented by cosine functions using the force constants, k_d, the harmonic coefficents, n_d, and the phase angles ω_d. The standard Lorentz-Berthelot mixing rules, $\varepsilon_{ij}=(\varepsilon_i\varepsilon_j)^{1/2}$ and $\sigma_i=(\sigma_i+\sigma_j)/2$, have been applied throughout this work.

The Antechamber software from AmberTools 1.4 was used to generate GAFF topologies, with the point charges derived through the AM1-BCC method. The GAFF topologies and coordinate files were converted into the GROMACS format using the ACPYPE script.[36]

The majority of the simulations of the bent-core mesogens were performed on 248 or 256 molecules. A cut-off of 1.2 nm was used for short range non bonded interactions, the Particle Mesh Ewald (PME) method was used for long-range electrostatics, and the simulations employed the usual corrections for the pressure and potential energies to compensate for the truncation of the vdW interactions. The Berendsen thermostat and barostat was used for initial simulation setups compressing, at 100 bar pressure, from low-density random arrangements of molecules, followed by equilibration and production runs with a Nose-Hoover thermo-

stat and Parrinello-Rahman barostat, once liquid state densities were reached. We used isotropic pressure coupling and a compressibility of 4.6×10^{-5} bar^{-1} throughout; noting that we saw no evidence of the directior of the system being influenced by any particular box vectors in the nematic phase. For one system (see below - section 3), where we see some form of translational order, we note that this is seen in a simulation box that is quite large (2048 molecules). Hence, we do not expect any periodicity to be imposed on the system by fixing the relative simulation box dimensions via isotropic pressure coupling. Bond lengths were kept fixed at their equilibrium values using the LINCS algorithm and a timestep of 2 fs was employed. Each system was progressively cooled at 10 K intervals, with equilibration runs of 60 ns followed by production runs ranging from 120 to 180ns. These lengthy simulation times, coupled with cooling the system from disordered configurations, provide greater confidence in the results when observing the spontaneous onset of ordering in LC phases.[2,20,37]

Larger systems were also investigated for two of the mesogens by replicating the smaller systems twice in each direction to give up to $N = 2048$ molecules. These were then re-equilibrated for 10 ns followed by production runs of a further 20 ns.

A small number of simulations of *n*-alkane molecules in the liquid phase were also carried out using 1000 molecules at 298 K and a pressure of 1 bar, using the procedure described above. Each production run was carried out for 20 ns The heat of vaporization was calculated using

$$\Delta_{\text{vap}}H = (E_{\text{pot}}(g) + k_B T) - E_{\text{pot}}(l), \tag{2}$$

where $E_{\text{pot}}(g)$ represents the intramolecular energy in the (ideal) gas phase and $E_{\text{pot}}(l)$ is the intermolecular energy in the liquid phase. The gas phase simulations, for one molecule, were performed using a stochastic dynamics (SD) integrator, which adds a friction and a noise term to Newton's equation of motion. Gas phase calculations were carried out over 200 ns.

Data Analysis

Molecular orientational order for the mesogens was monitored through the calculation of the uniaxial order parameter, S_2. This was obtained through diagonalization of the ordering matrix, $\mathbf{Q}$, defined as

$$\mathbf{Q}_{\alpha\beta}(t) = \frac{1}{2N}\sum_{i=1}^{N}\left[3u_{i\alpha}u_{i\beta} - \delta_{\alpha\beta}\right], \ \alpha,\beta = x,y,z, \tag{3}$$

where the sum runs over all N molecules. The largest eigenvalue of the $\mathbf{Q}$ tensor represents S_2 and the associated eigenvector represents the phase director, $\mathbf{n}$. However, in order to minimise system size effects in locating the phase transition, we use $-2\times$ the middle eigenvalue of $\mathbf{Q}$, which fluctuates about a value of zero in the isotropic phase but equals $S_2(t)$ in the nematic phase. Typically, S_2 was defined as the time average of $S_2(t)$, over the final 60 ns of the production runs.

Two definitions of the molecular long axis, were defined. One used the direction of the eigenvector corresponding to the minimum eigenvalue obtained through diagonalization of the molecular moment of inertia tensor. A second reference axis was defined as a vector parallel to the long axis of the aromatic core (Ph-ODBP-Ph). This was obtained by calculating vectors along the two arms of the bent core up to carbon atoms adjacent to the alkyl/alkoxy tails of the outer phenyl rings and subtracting one arm vector from the other to generate the core axis vector (see axis 1 in Fig. 1). In order to make comparisons with the experimentally measured uniaxial order parameters, a molecular reference axis parallel with one arm of the aromatic core was used in a small number of calculations.

Structural information in the liquid crystal phases was deduced by evaluating the pair distribution function: $g(r)$, which calculates probability of finding a particle at a distance, r, away from a given reference particle, relative to that for an ideal gas, regardless of particle orientation

$$g(r) = \frac{V}{N^2}\left\langle \sum_{i}^{N}\sum_{i\neq j}^{N}\delta(\mathbf{r} - \mathbf{r}_{ij})\right\rangle, \tag{4}$$

where $\mathbf{r}_{ij}$ is the vector between the centres of mass of two molecules i and j. In addition, $g(r)$ was resolved into two components, $g_{\parallel}(r)$ and $g_{\perp}(r)$, which can be used to monitor translational order parallel and perpendicular to the director respectively.

For $g_{\parallel}(r)$, we take distances, r_{ij}, between molecular centres resolved parallel to the director, i.e. $r = r_{\parallel} = \mathbf{r}_{ij}\cdot\mathbf{n}$, and calculate

$$g_{\parallel}(r) = \frac{\rho(r)}{\rho_{\text{bulk}}} = \frac{n(r)}{\rho_{\text{bulk}}V_{\text{shell}}} = \frac{n(r)}{\rho_{\text{bulk}}2\pi r_w^2 dr_{\parallel}}, \tag{5}$$

where $\rho_{\text{bulk}} = N/V$ is the mean number density of molecules in the system and $n(r)$ is the mean number of molecules in the volume contained by two disks each of height, $dr_{\parallel}$, and radius, $r_w = (r_{\text{cut}}^2 - r_{\parallel}^2)^{1/2}$ at distances $r = \pm|r_{\parallel}|$ (see Fig. S2). r_{cut} is the cutoff used in calculating the distribution function and must be less than half the length of the shortest simulation box size.

Likewise for $g_{\perp}(r)$, we resolve molecular centre-centre distances perpendicular to the director, $r = r_{\perp} = (r_{ij}^2 - r_{\parallel}^2)^{1/2}$ and calculate

$$g_{\perp}(r) = \frac{\rho(r)}{\rho_{\text{bulk}}} = \frac{n(r)}{\rho_{\text{bulk}}V_{\text{shell}}} = \frac{n(r)}{\rho_{\text{bulk}}2\pi h r_{\perp} dr_{\perp}}, \tag{6}$$

where $n(r)$ is the mean number of molecules contained in the volume of a cylindrical shell centred at, $r = r_{\perp}$ with a width of $dr_{\perp}$, and a height, $h = 2(r_{\text{cut}}^2 - r_{\perp}^2)^{1/2}$ (see Fig. S2).

The molecular dimensions were quantified through considering the average moment of inertia tensor, $\langle I\rangle$ where $\langle I_1\rangle$, $\langle I_2\rangle$ and $\langle I_3\rangle$ are the averaged principle moments of inertia. These values enable the average length, $2a$, width, $2b$, and breadth, $2c$, of a mesogen to be calculated using $a = \sqrt{2.5(I_2 + I_3 - I_1)m}$ and cyclic permutations for b and c.[38]

Results and Discussion

Additional improvements to the GAFF force field

We used the GAFF-LCFF improvements to the original GAFF force field, as developed in our previous work.[11] However, due to the specific chemical details of the bent-core mesogens studied in

Table 1 Density and heat of vaporization calculations for various *n*-alkanes using GAFF and GAFFlipid. [a]All values at 298 K. [b]Data taken from the CRC Handbook of Chemistry and Physics.[39] [c] Data taken from ref.[40] [d] GAFFlipid with LJ parameters modified.

n -alkane	Property[a]	Exp.[b]	GAFF	GAFFlipid	GAFFlipid (modified)[d]
Pentadecane	Density / g cm^{-3})	0.7690	0.8420[c]	0.7510[c]	-
	Heat of Vap. / kJ mol^{-1}	76.77	105.88[c]	77.01[c]	-
Dodecane	Density / g cm^{-3})	0.7495	0.8240 $\pm$ 0.0003	0.7450 $\pm$ 0.0002	-
	Heat of Vap. / kJ mol^{-1}	61.52	96.21 $\pm$ 0.10	56.02 $\pm$ 0.05	-
Heptane	Density / g cm^{-3})	0.6795	0.6782 $\pm$ 0.0001	0.6637 $\pm$ 0.0002	0.6819 $\pm$ 0.0001
	Heat of Vap. / kJ mol^{-1}	36.57	40.37 $\pm$ 0.03	31.80 $\pm$ 0.05	35.70 $\pm$ 0.01
Pentane	Density / g cm^{-3})	0.6260	0.6132 $\pm$ 0.0001	0.5865 $\pm$ 0.0002	0.6119 $\pm$ 0.0002
	Heat of Vap. / kJ mol^{-1}	26.43	28.45 $\pm$ 0.02	21.98 $\pm$ 0.01	25.13 $\pm$ 0.02

this work, additional parameter refinements were needed to enhance GAFF-LCFF. This included examination of the ring-chain torsion, specifically as the bent-core mesogens studied here contained a mixture of either alkyl or alkoxy terminal chains attached to the rigid core. An accurate description of the ring-chain torsion is considered to be an important feature in reproducing correct mesophase behaviour as specific orientations at this junction are important in establishing the overall mesogen shape.[41]

NMR experimental studies and DFT calculations of the alkyl-ring junction in ethylbenzene predict minima when the $C_{ca}-CH_2$ bond is in the plane perpendicular ($\pm 90^\circ$) to the ring.[14,42] Likewise, minima at $\pm 90^\circ$ are also predicted from NMR studies for the analogous bond in the 4CB mesogen.[42] There is some uncertainty in the literature concerning the barrier to rotation about the $C_{ca}-CH_2$ bond. A DFT calculation at the B3LYP/6-311+G(2dp) level of theory for ethylbenzene yielded a barrier height of 4.5 kJ mol^{-1} at 0°, whereas that obtained from NMR data was $\approx$ 3 kJ mol^{-1}.[14] A significantly larger barrier height of $>$ 22 kJ mol^{-1} obtained from NMR data is found for the $C_{ca}-CH_2$ torsion of the 4CB mesogen,[42] indicating a possible problem of parameter transferability from small fragments to larger molecules for this particular torsion. The original GAFF force field was tested on the analogous torsion of butylbenzene and predicted minima at $\pm 90^\circ$, and a barrier height of $\approx$ 12 kJ mol^{-1}. Due to the range of values found for the barrier to rotation about the $C_{ca}-CH_2$ bond depending on the molecular context, it was decided to retain the original GAFF Ryckaert Belleman (RB) coefficients for this torsion, particularly as the correct minimum geometry was predicted.

According to theoretical results, and in contrast to the $C_{ca}-CH_2$ torsion, the torsional potential for $C_{ca}-OCH_2$ has two equivalent minima corresponding to the O-CH_2 bond lying in the same plane as that of the aromatic ring.[43,44] An extensive *ab initio* approach, employing MP2, MP3, MP4(SDQ), CCSD and CCSD(T), yielded a barrier height of $\approx$ 12.5 kJ mol^{-1} for the $C_{ca}-OCH_2$ torsion of the methoxybenzene,[43] while for the analogous torsion of ethoxybenzene, a barrier height of $\approx$ 11 kJ mol^{-1} was obtained employing DFT at the B3LYP/6-311+G(2dp) level of theory.[41] A slightly greater barrier height of $\approx$ 18 kJ mol^{-1} employing B3LYP/6-31G(d) was calculated for the $C_{ca}-OCH_2$ torsion of a series of bent-core mesogens containing alkoxy chains of various lengths, although this value was dependent on the type of group connected to the *para* position of the ring with respect to the chain.[44] Noting that the small basis set, and absence of diffuse functions, may have reduced the accuracy of the calculations. The original GAFF force field produced the correct minimum energy geometry for the $C_{ca}-OCH_2$ torsion of ethoxybenzene, but a barrier height of $\approx$ 2.5 kJ mol^{-1}, significantly lower than literature values. New RB coefficients, C_n were obtained to replicate the torsional barrier of $\approx$ 11 kJ mol^{-1} derived from the literature DFT calculations at a B3LYP/6-311+G(2dp) level of theory and these were transferred to the analogous dihedrals in the bent-core mesogens.

Initial test simulations using GAFF-LCFF provided good estimates of the experimental T_{NI} temperatures for the C4O-Ph-ODBP and C4O-Ph-ODBP(trimethylated) mesogens. However, for the longer chained C4-Ph-ODBP-Ph-C7 and C5-Ph-ODBP-Ph-OC12 mesogens the T_{NI} estimates were $\approx$ 20 to 30 K higher than experimental values, which although a significant improvement on the original GAFF predictions suggested there was still room for improvement. A study by Dickson *et al.*[40] employing GAFF for the simulations of lipid bilayers found that GAFF considerably overestimates both density and $\Delta_{vap}H$ for long hydrocarbons compared with experimental values. These authors tuned the carbon and hydrogen LJ parameters in order to replicate more accurately the experimental properties of simple hydrocarbons. In addition, the C$-$C$-$C$-$C torsion was corrected and fitted to the high level QM calculation, MP4/6-311G(d,p)//MP2/6-31G* and introduced into the force field (GAFFlipid force field) which had the effect of reducing the *t/g* energy difference as well as the *trans-gauche* (*t-g*) barrier.

The original GAFF predictions for both density and $\Delta_{vap}H$ for butane were found to be in good agreement with experimental values ($<$ 3 %).[45] However, for medium to long *n*-alkanes the discrepancy between calculated and experimental values increases with increasing chain length (see Table 1). In particular, the calculated $\Delta_{vap}H$ values for pentadodecane and dodecane are particularly poor and the densities are $\approx$ 10 % greater than experimental values. Although the calculated densities for the smaller alkanes, pentane and heptane, are reasonably good, the $\Delta_{vap}H$ values are still $\approx$ 8 to 10 % greater than experimental values. It was therefore considered that the varying length carbon chains of the bent-core mesogens, in particular the C5, C7 and C12 chains, may require refinement of the LJ parameters. This was also thought to be the most likely explanation for the slightly overestimated T_{NI} temperatures for C4-Ph-ODBP-Ph-C7 and C5-Ph-ODBP-Ph-OC12

mesogens with the GAFF-LCFF force field.

The GAFFlipid LJ carbon and hydrogen parameters, along with the GAFFlipid C−C−C−C torsional parameters, were tested on dodecane (C12), heptane (C7) and pentane (C5). The results for the reproduction of experimental data are shown in column 5 of Table 1, along with the results for pentadecane (C15), taken from the original development of GAFFlipid.[40] These results indicate that the estimates of the experimental properties, in particular the $\Delta_{vap}H$ values for longer *n*-alkanes, are significantly improved with the GAFFlipid force field. However, for the shorter chains, heptane and pentane, the originally overestimated $\Delta_{vap}H$ values are significantly underestimated compared with experimental values, along with a small underprediction of densities. The best results for heptane and pentane were obtained through a small modification to the GAFFlipid LJ parameters. It was found that multiplying the difference between original GAFF and GAFFlipid LJ parameters by 0.75 produced the best overall results for both these properties.

To verify that the inclusion of GAFFlipid torsional parameters in conjunction with the adopted/amended GAFFlipid LJ parameters reduced the *t/g* energy difference *n*-alkanes of various length, the torsional profiles for the first C−C−C−C dihedral of both dodecane and pentane were calculated. A small reduction in both these values is apparent compared with the original GAFF values (see Fig. 2). In the previous study, developing GAFF for liquid crystals,[11] a similar reduction in the *t/g* energy difference was obtained through incorporating Sui *et al.*[46] C−C−C−C torsional parameters, developed for the OPLS force field. However, it was considered that the GAFFlipid approach had the added advantage of addressing the need to amend the LJ parameters (particularly for longer *n*-alkanes) as well as refinement of the C−C−C−C torsional parameters.

Due to the fact that GAFF only assigns single atom types to the carbon and hydrogen atoms of carbon chains, it was not possible to differentiate the LJ parameters on differing length chains of the unsymmetrical bent-core ODBP mesogens. Therefore it was decided to adopt the GAFFlipid LJ parameters for both the hydrocarbon chains of the C5-Ph-ODBP-Ph-OC12 mesogen, but for the C4-Ph-ODBP-Ph-C7 mesogen, the modified GAFFlipid LJ parameters were used. For the C4O-Ph-ODBP and C4O-Ph-ODBP(trimethylated) mesogens, containing very short C4 carbon chains, the original GAFF LJ parameters were retained. In all cases the C−C−C−C torsional parameters were adopted from the GAFFlipid force field. All new parameters derived for GAFF-LCFF, from this work as well as from the previous study, are shown in Tables S1 and S2 in the supplementary information.

The nematic to isotropic transition for C5-Ph-ODBP-Ph-OC12

The location of a NI phase transition can be determined by analysing the temperature variation of the uniaxial orientational order parameter, S_2. Fig. 3 shows the temperature dependent S_2 values averaged over the last 60 ns of the production runs for the C5-Ph-ODBP-Ph-OC12 system. These are plotted for different choices of the molecular reference axis (see Fig.1). To assess system size effects, the $\langle S_2 \rangle$ values for a $N = 2048$ sample size (axis 1) for selected temperatures are also shown for comparison, with results given as average values calculated over 20 ns production runs. Following the criteria established in references[2,21], T_{NI} is considered to be the highest temperature at which $\langle S_2 \rangle$ is larger than 0.15.

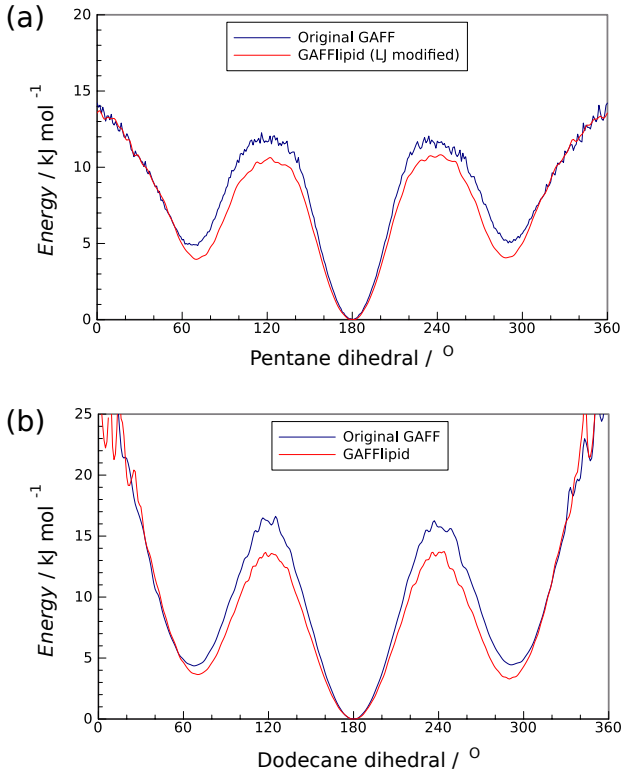

Fig. 2 Effective torsional potentials for the first dihedral of pentane and dodecane obtained by Boltzmann inversion of dihedrals angle distributions, derived from gas-phase simulations.

The $\langle S_2 \rangle$ values calculated for the long axis of the core (axis 1) and the inertia axis for the $N = 256$ sample size are almost identical, suggesting that the uniaxial ordering of the core is imposed on the entire molecule. This observation is also consistent with the $\langle S_2 \rangle$ measurements obtained by Pelaez and Wilson[47] for the ODBP-Ph-C7 mesogen, the only other fully atomistic simulation of an ODBP based bent-core mesogen, as far as the authors are aware. At the higher temperatures of 530 and 520 K, $\langle S_2 \rangle$ values for these axes assume effectively isotropic values of $<$ 0.15. At 510 K $\langle S_2 \rangle$ increases to just above 0.2, indicating a weak first-order transition at this temperature. This is also supported by observing the evolution of the instantaneous value of S_2 as a function of time for temperatures close to the phase transition (see Fig. 3b). At 520 K and 510 K, S_2 shows progressively larger fluctuations between the ordered and disordered state. However, upon cooling the system to 500 K, S_2 shows smaller fluctuations and assumes an average value of 0.43 over the last 120 ns, which is typical of a nematic phase. These results suggest a simulated T_{NI} of $\approx$ 510 K, which is in excellent agreement with the experimental T_{NI} of 512 K.

The larger $N = 2048$ system shows a small reduction in $\langle S_2 \rangle$ values compared with those calculated for the $N = 256$ system

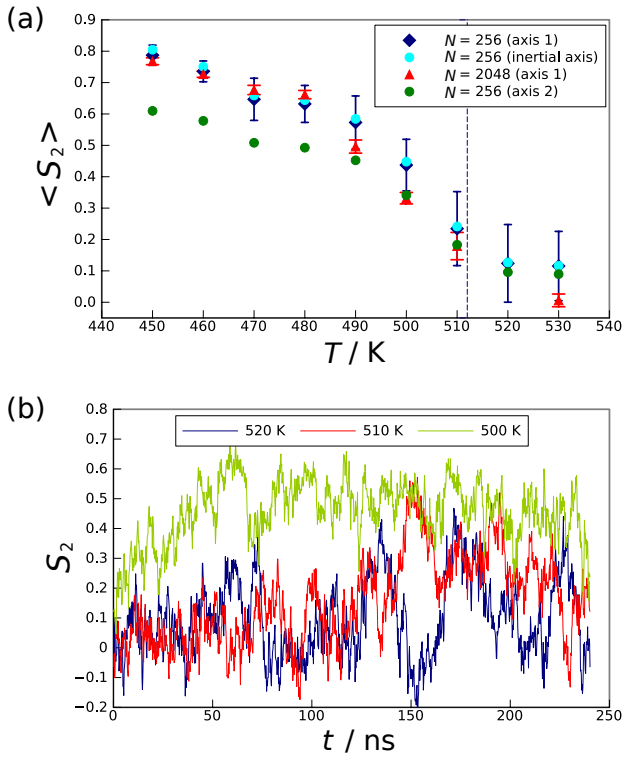

Fig. 3 (a) Average uniaxial order parameters as a function of temperature for C5-Ph-ODBP-Ph-OC12 and N = 256 and N = 2048 systems. (The dotted line represents the experimental T_{NI}. Typical error bars are shown for one data set based on the standard deviation of S_2.) (b) Order parameter as a function of time at temperatures close to the phase transition. (N = 256 molecules and for axis 1)

and for the molecular reference axes described above, with these differences more pronounced in the isotropic phase and at higher temperatures in the nematic phase. However, the $\langle S_2 \rangle$ at 510 K was calculated to be $\approx$ 0.18, again indicating a simulated T_{NI} in the vicinity of this temperature. Limited system size effects have been noted for other atomistic simulations of different liquid crystal molecules. For example, a reduction of $\approx$ 15 K was found in the simulated T_{NI} temperature for a linear oligothiophene based mesogen when increasing the sample size from 140 to 1120 molecules,[7] and Palermo *et al.*[37] found a reduction of $\approx$ 5 K in the simulated T_{NI} temperature of 8CB when increasing the sample size from 250 to 750 molecules. In contrast to these results, Zhang *et al.*[20] found no size dependence with regard to the T_{NI} temperatures for both 5CB and 8CB and stated that a system size N = 256 molecules was sufficient to yield thermodynamic, structural and dynamic properties for these specific systems.

Finally, due to the unique shape of bent-core mesogens, $\langle S_2 \rangle$ was also calculated for molecular reference axis 2 (as defined in figure 1), parallel with one arm only and for the N = 256 sample size. The results plotted in Fig. 3 show systematically lower $\langle S_2 \rangle$ values, in particular at the higher nematic temperature region compared with those calculated for the other reference axes, including the N = 2048 sample size. Although the location of the simulated T_{NI} is approximately the same.

Uniaxial orientational order parameters have been experimentally determined for the C5-Ph-ODBP-Ph-OC12 system, employing Polarized Raman Scattering (PRS).[34,48] In this case two different models were considered in the analysis of the data. One model monitored the intensity of the Raman scattered light (phenyl stretching mode) from one arm only and the second model considered the effect of the molecular bend angle through analysis of the Raman scattered light from both arms and summing the electric field contributions from each arm. This latter model assumed a fixed molecular bend angle of 140°. Their results showed systematically lower $\langle P_{200} \rangle$ values for the model which took no account of the bend angle (one scatterer) compared with the model that included a molecular bend angle (two scatterers).

In the current study, the simulated $\langle S_2 \rangle$ values calculated for the molecular reference axes 1 and 2 show good agreement with the experimental data (see $\langle P_{200} \rangle$ values in Figure 1 of reference[48]) although some caution needs to be applied in making direct comparisons with the experimental results, due to the fitting procedure employed and the explicit use of a fixed bend angle parameter in one of the models in the Raman scattering study.

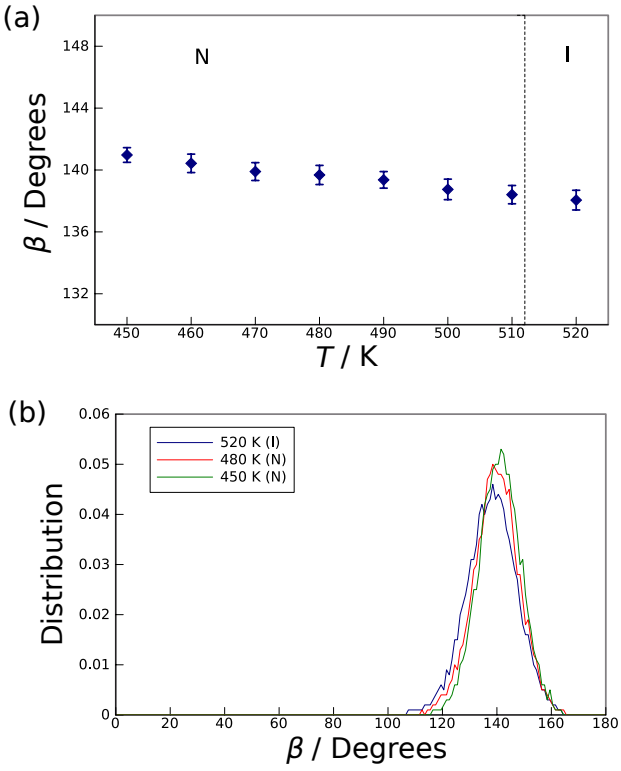

Fig. 4 (a) The average bend angle of the Ph-ODBP-Ph core of C5-Ph-ODBP-Ph-OC12 as a function of temperature. (Error bars are shown based on the standard deviation of β.) (b) Distribution of the bend angle in the simulated phases.

A number of issues concerning the interpretation of Raman scattering data and the measurement of orientational order parameters for bent-core nematics have been raised, in particular, whether the inclusion of the molecular bend angle in the deduction of the order parameters is necessary, and if so, whether the bend angle is temperature dependent or not. For example, Park *et al.*'s Raman scattering measurements of uniaxial order parame-

ters for a different bent-core nematic show identical $\langle P_{200} \rangle$ values regardless of whether the Raman scattering data is analyzed with respect to one arm only, or to both of the arms.[49] Park *et al.* suggest that consideration of the bend angle in the measurement of order parameters is not important, as rotational freedom in the nematic phase would average out the influence of the bent shape, and even if it was important, then the influence of temperature on the value of the angle would need to be tested. However, Southern *et al.* state that accounting for a temperature independent fixed molecular bend angle in the analysis of the data is necessary and have also reported $\langle P_{200} \rangle$ and $\langle P_{400} \rangle$ values for five additional ODBP compounds using this model, which they claim are in excellent agreement with theory.[50]

The average bend angle, β, was calculated as the angle between two vectors parallel to the arms of the Ph-ODBP-Ph core. The temperature dependence of β is shown in Fig. 4a. The results show that in the nematic phase, $<\beta>$ increases by as little as 2.6° with decreasing temperature. In addition, the distribution of angles are narrow and broadly similar for selected simulated temperatures, with peak values occurring at $\approx$ 140°, (see Fig. 4b). These results support the assumption that a temperature independent (fixed bend angle) is justified in the analysis of Raman scattering data and in the determination of uniaxial order parameters for the C5-Ph-ODBP-Ph-OC12 system.[34]

The nematic to dark conglomerate (DC) transition for C5-Ph-ODBP-Ph-OC12

The dark conglomerate phase formed by achiral bent-core liquid crystals is generally described as a spontaneously chiral, isotropic fluid, characterized by local deformed smectic layering.[51] A number of different DC phases have been identified depending on the local structure.[52,53] For the C5-Ph-ODBP-Ph-OC12 system, observations by polarizing optical microscopy show a transition to a DC phase directly below the nematic phase.[54] This is in contrast to other bent-core materials possessing a DC phase, for which this phase occurs directly below the high-temperature isotropic phase.[51,55] The internal structure of the DC phase of C5-Ph-ODBP-Ph-OC12 has been reported to consist of tilted polar smectic layers with relatively short correlation length, with these layers curving continuously forming a saddle type structure. In the ground state the orientation of the tilt and polarity is antiparallel ($\mathrm{Sm}C_AP_A$).[56] The strong tendency for saddle-splay layer deformation has been attributed to the projection of the tilt direction of each molecular arm onto the layer plane, which is almost perpendicular. This leads to dilation in one half-layer (containing one arm) and compression in the other half-layer producing a frustrated state that can only be relieved by saddle-splay curvature.[51,55]

Figure 5 shows snapshots of the simulations of C5-Ph-ODBP-Ph-OC12 cooled down to 430 K. For clarity, only the simplified ODBP bent-core structures are shown. Visual observations of the system at 460 K indicate a broadly homogeneous nematic state, with long-range order of the molecular long axes, and no indication of smectic-like layers. Cooling the system to 450 K shows increasing segregation of the ODBP cores with respect to the alkyl tails, and the emergence of ribbon or wave-like structures, suggesting some degree of pretransitional molecular organization at this temperature. At 430 K the molecular organization appears considerably more ordered, with the presence of distinct layers which appear distorted and splayed from certain perspectives (See Fig. 5c). It is likely that at this temperature, the system is exhibiting the expected DC phase which has been observed and characterized experimentally.[56]

To obtain more information on the mesophase structures of the the C5-Ph-ODBP-Ph-OC12 system, various pair distributions were evaluated. Fig. 6a shows $g(r)$ calculated with respect to the centre of the oxadiazole ring and for temperatures in the nematic phase and the expected DC phase. The profiles of $g(r)$ clearly show no sharp peaks in the medium to long range (characteristic of smectic structure) and, with the exception of 430 K, quickly decay to the asymptotic value of 1. The initial split peak, which grows with decreasing temperature, indicates some weak correlation between neighbouring molecules, and this becomes stronger as the system is cooled.

As visual observations of the system at the lower temperatures of 450 K down to 430 K indicate unusual nanostructures and layer-like mesogenic organization, $g(r)$ was resolved into two components, $g_{\parallel}(r)$ and $g_{\perp}(r)$, which can be used to monitor translational order parallel and perpendicular to the director (See Fig. 6b and c). The profiles of both $g_{\parallel}(r)$ and $g_{\perp}(r)$ for all the temperatures, including 430 K, are largely featureless with negligible structure at all values of r. In particular, the absence of well defined oscillatory peaks in $g_{\parallel}(r)$ at the lower temperatures (450 to 430 K) suggests an absence of translational ordering and hence an absence of repeating mesogenic layers. These results are therefore not consistent with the emergence of a standard smectic phase below the nematic region.

To gain further insight into the nature of the "layer order" within the DC phase, two additional pair distribution functions denoted $g(d_{\parallel})$ and $g(d_{\perp})$ were calculated. Unlike $g_{\parallel}(r)$ and $g_{\perp}(r)$, which use components of the intermolecular vectors relative to the average molecular direction (i.e. the system director), these distribution functions enabled the intermolecular vectors (represented as the distances between molecular centres of mass) to be analyzed relative to the instantaneous orientation of each molecule (represented by the orientation of axis 1 in Fig. 1). The distances, $d_{\parallel}$ and $d_{\perp}$ are taken from the vectors $\mathbf{d}_{\parallel}^{ij}$ and $\mathbf{d}_{\perp}^{ij}$ for all $i \neq j$. $\mathbf{d}_{\parallel}^{ij} (\neq \mathbf{d}_{\parallel}^{ji})$ is the projection of the intermolecular vector $\mathbf{d}_{ij} = \mathbf{d}_i - \mathbf{d}_j$ onto the axis vector of the molecular core (axis 1) and $\mathbf{d}_{\perp}^{ij}$ is the projection of $\mathbf{d}_{ij}$ onto the plane perpendicular to $\mathbf{d}_{\parallel}^{ij}$. The following results (Fig. 7) are for the temperatures 460 K down to 430 K, representing the lower nematic region, the pretransitional region of the DC phase and the DC phase itself.

It is immediately apparent that the profiles for both of these pair distribution functions (Fig. 7a and b) indicate more structure compared with those shown in Fig. 6b and c. For example, at T = 460, 450 and 440 K, $g(d_{\parallel})$ shows an initial contact peak followed by a very weak secondary peak at $\approx$ 41 Å, after which the correlation functions decay to unity. The amplitude of the secondary peak indicates that in the vicinity of one molecular

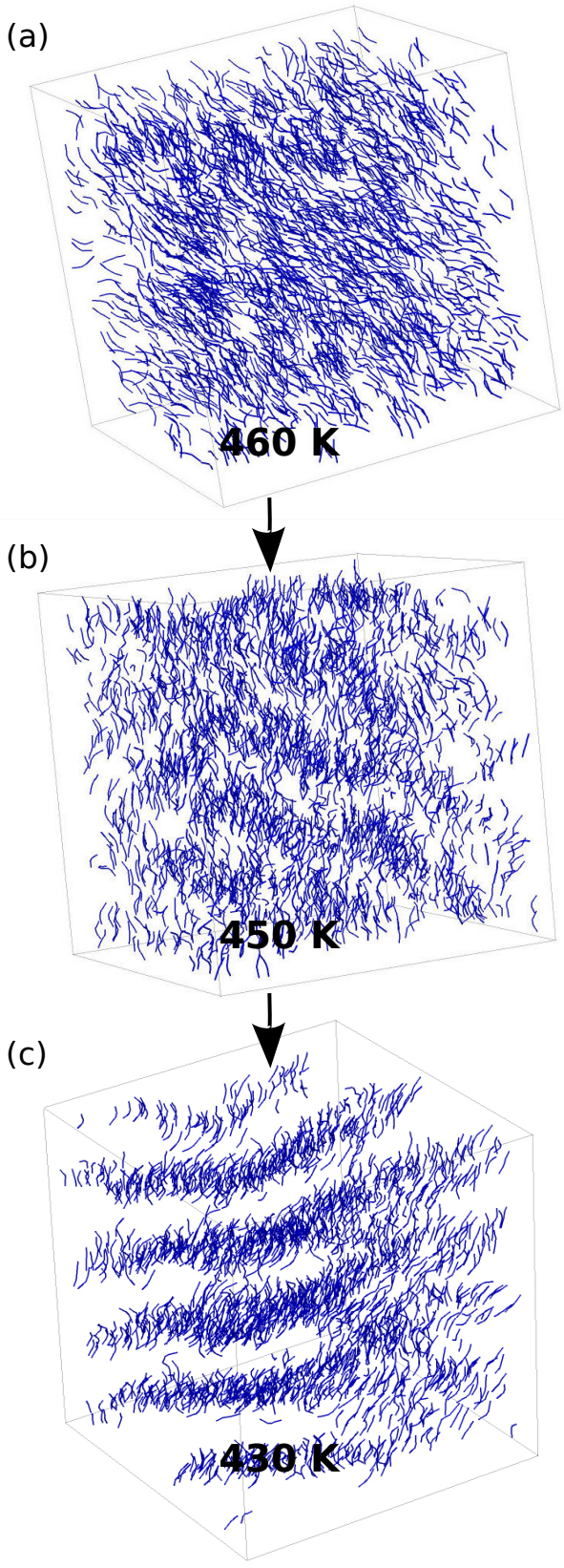

Fig. 5 Snapshots of the C5-Ph-ODBP-Ph-OC12 system cooled down to 430 K (N = 2048 molecules and simulation box size = (125 Å)^3).

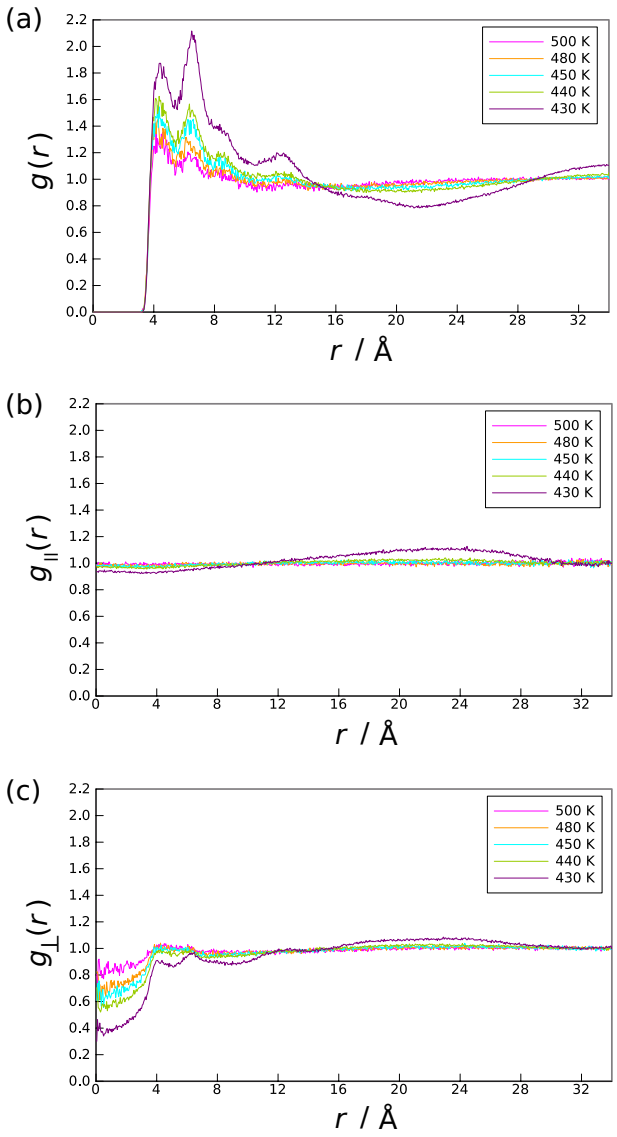

Fig. 6 Pair distribution functions as a function of temperature for C5-Ph-ODBP-Ph-OC12 (a) $g(r)$ (b) $g_{\parallel}(r)$ and (c) $g_{\perp}(r)$

length and in the direction parallel to the long axis of the ODBP core, there is only a very weak tendency for the molecules to arrange into layers. At T = 430 K, however, $g(d_{\parallel})$ shows a more pronounced initial and secondary peak before appearing to decay to unity, suggesting greater positional order and a stronger local preference for arranging into layers. The distance at which the secondary peak occurs ($\approx$ 41 Å) corresponds to a distance which is less than the average molecular length deduced from the simulations, which in the nematic phase shows a small increase from $\approx$ 46.8 to 48.9 Å with decreasing temperature. This indicates there is some degree of intercalation of the alkyl chains and/or tilting of the ODBP cores.

The results for $g(d_{\perp})$ at T = 460, 450 and 440 K (Fig. 7b) show a strong initial peak, corresponding to nearest neighbour molecules, followed by an absence of discernible longer range peaks. The profiles for $g(d_{\perp})$ are very similar in each case, with the transverse correlation lengths $\leq$ 16 Å. In contrast, at T =

430 K, there is a significant difference in the profile of $g(d_\perp)$ with the appearance of well defined peaks and a transverse correlation length of at least 60 Å.

The change in the profiles of both $g(d_\parallel)$ and $g(d_\perp)$ at 430 K, suggests the presence of a significantly more structured phase at this temperature although the results do not support the presence of a typical smectic phase, as smectic ordering appears to be more local and the intermolecular correlation length relatively short. This, in conjunction with the visual observations of the system at 430 K, indicates the presence of curved layers consistent with the saddle-splay curvature expected within a DC phase. However, an estimate of a simulated phase transition temperature (eg. $T_{\text{N-DC}}$) is rather difficult. For example, it is evident from viewing the snapshots of the system at 450 K, that there is a distinct change in the nanostructure from that of a typical nematic, although this is not corroborated by the behaviour of the various pair distribution functions. It is possible that a phase transition into a more ordered phase occurs somewhere between 450 and 430 K, which is a little lower than the experimentally determined $T_{\text{N-DC}}$ of 458 K.

The importance of understanding the general structure property relationships of mesogens capable of forming DC phases is important for developing these interesting materials for technological applications.[52,57] It is curious that the three ODBP bent-core mesogens reported in the following section do not display a DC phase, suggesting that chemical and structural features specific to the C5-Ph-ODBP-Ph-OC12 mesogen are necessary for the promotion of a DC phase for this system. The combination of both alkyl and alkoxy terminal chains in the C5-Ph-ODBP-Ph-OC12 mesogen lead to differing core-chain topologies, which in turn may affect the packing densities of the mesogens resulting in specific mesophase structures.

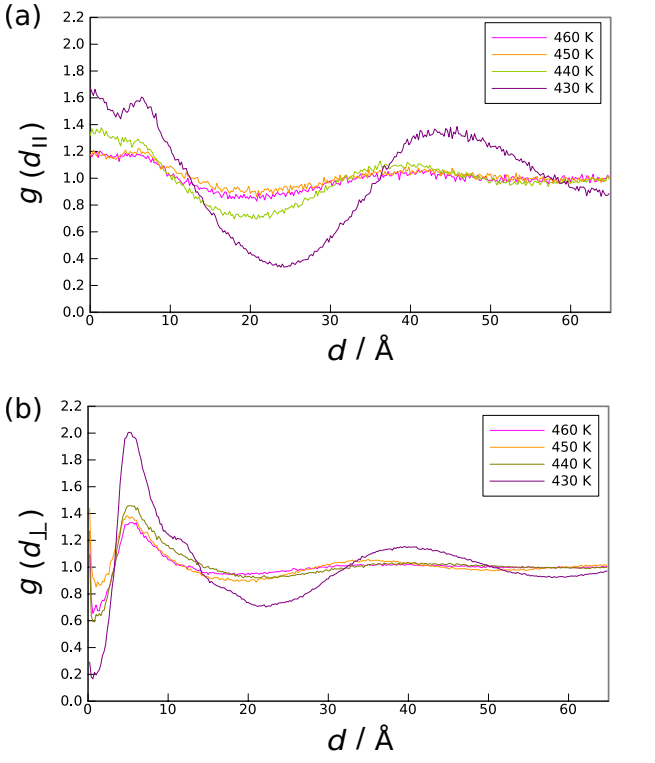

Fig. 7 Pair distribution functions as a function of temperature for C5-Ph-ODBP-Ph-OC12 (a) $g(d_\parallel)$ and (b) $g(d_\perp)$

The NI Phase Transitions of the C4-Ph-ODBP-Ph-C7, C4O-Ph-ODBP and C4O-Ph-ODBP(trimethylated) mesogens

The optimized force field (GAFF-LCFF) was further tested on its ability to reproduce the experimental NI transitions of three additional ODBP bent-core mesogens (see Fig. 1). The location of the NI transitions were deduced from analysis of the temperature behaviour of the order parameter, S_2, calculated for a vector parallel with the long axis of the aromatic core of each molecule as defined for the C5-Ph-ODBP-Ph-OC12 system described previously. However, unlike C5-Ph-ODBP-Ph-OC12, comparison of the simulated S_2 values with experimentally determined uniaxial order parameters was not possible due to the absence of any experimental order parameter data for these systems.

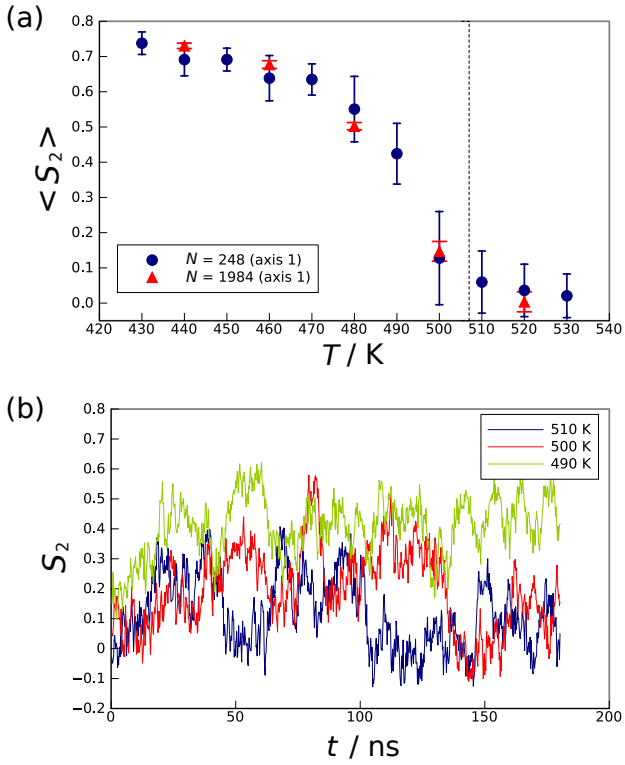

Fig. 8 (a) Average uniaxial order parameters as a function of temperature for the C4-Ph-ODBP-Ph-C7 system. (The dotted line represents the experimental T_{NI}. Error bars are shown based on the standard deviation of S_2.) (b) Order parameter as a function of time at temperatures close to the phase transition. (N = 248 molecules)

Figure 8a shows $\langle S_2 \rangle$, averaged over the final 60 ns of the production runs for the C4-Ph-ODBP-Ph-C7 system and for N= 248 molecules. At the temperatures 530, 520 and 510 K, $\langle S_2 \rangle$ assumes isotropic values of < 0.1. A small increase in $\langle S_2 \rangle$ to ≈ 0.15 is observed at 500 K followed by a larger increase to ≈ 0.4 at 490 K. The highest temperature at which $\langle S_2 \rangle$ is greater than 0.15, defined as the simulated T_{NI} , is therefore 490 K. However, examination of the time evolution of the order parameter over the full trajectory for the small system size (see Fig. 8b) indicates that at

510 K the system is approaching a phase transition with $S_2(t)$ displaying oscillations in its value. At 500 K, larger long-time scale fluctuations in S_2 are observed. When averaged over the full trajectory, these give a $\langle S_2 \rangle$ value of ≈ 0.2, higher than the average value for the final 60 ns of the production runs shown in Figure 8a. This provides an estimate of the simulated T_{NI} of ≈ 500 K which is in reasonable agreement with the experimental value of 507 K.

System size effects were also tested for a selection of temperatures and were found to be relatively insignificant, with little differences in these values or in the location of the phase transition temperature (see Fig. 8a).

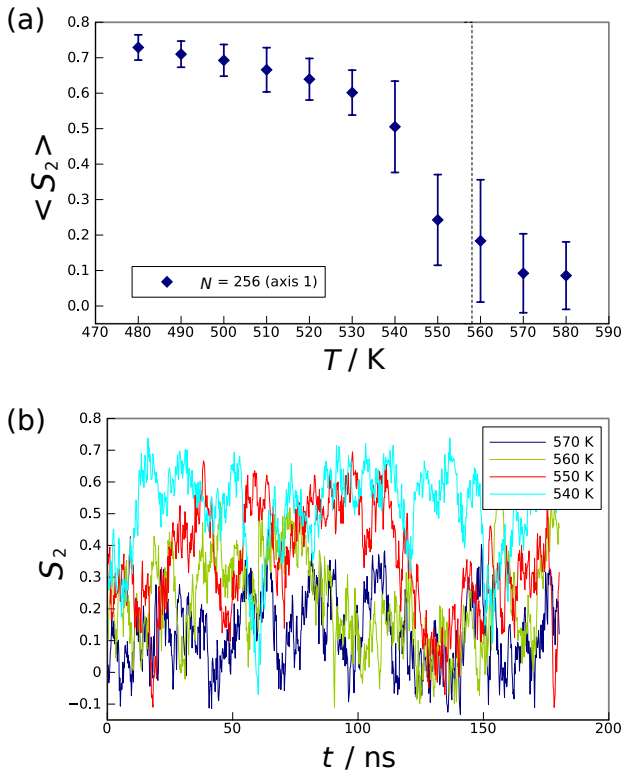

Fig. 9 Average uniaxial order parameters as a function of temperature for the C4O-Ph-ODBP system. (The dotted line represents the experimental T_{NI}. Error bars are shown based on the standard deviation of S_2.) (b) Order parameter as a function of time at temperatures close to the phase transition. (N = 256 molecules)

Fig. 9a shows the temperature dependent uniaxial order parameters, $\langle S_2 \rangle$, averaged over the final 60 ns of the production runs for the C4O-Ph-ODBP system. For C4O-Ph-ODBP it was assumed that a sample size of N= 256 molecules was sufficient for locating the NI transition temperature, due to the lack of any significant size dependence of this property for the previously discussed ODBP mesogens.

Isotropic values of the order parameters ($\langle S_2 \rangle < 0.1$) are observed at 570 K and above. A small jump in the value of $\langle S_2 \rangle$ to ≈ 0.18 occurs at 560 K, providing an estimate of the simulated T_{NI}. However, further information on the location of the simulated T_{NI} is provided by examination of the time evolution of S_2 at temperatures close to the phase transition (see Fig. 9b). Large fluctuations in S_2 are observed at both 560 and 550 K which lead to large standard deviations in $\langle S_2 \rangle$. This behaviour is expected when approaching the transition temperature both from the isotropic and from the nematic side and is consistent with the weakly first-order nature of the transition.[2,37] These results therefore indicate a simulated T_{NI} somewhere between 560 and 550 K which is in very good agreement with the experimental value of 558 K.

In contrast to the non-methylated ODBP mesogens, C4O-Ph-ODBP(trimethylated) shows a much reduced nematic onset temperature as well as a nematic phase that can be supercooled down to room temperature. In addition, unusual wide-angle XRD data has also been observed for this mesogen which is absent for the non-methylated ODBP bent-core mesogens discussed in this paper, or for the majority of bent-core systems. This has been attributed to a higher degree of local biaxial order, possibly due to the methyl substituents on the outer phenyl rings of the aromatic core.[3,33]

Fig. 10a shows shows S_2 values calculated for the C4O-Ph-ODBP(trimethylated) mesogen as a function of decreasing temperature and averaged over the final 60 ns of production runs. The temperatures extend down to room temperature (≈ 300 K) to include the expected supercooled nematic region for this system.

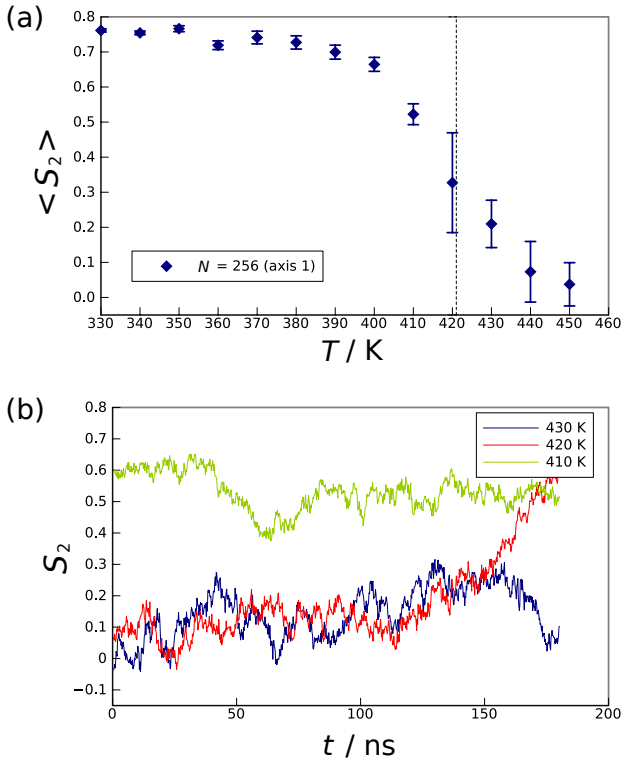

Fig. 10 Average uniaxial order parameters as a function of temperature for the C4O-Ph-ODBP(trimethylated) system. (The dotted line represents the experimental T_{NI}. Error bars are shown based on the standard deviation of S_2.) (b) Order parameter as a function of time at temperatures close to the phase transition. (N = 256 molecules)

Above 430 K, the system appears isotropic with $\langle S_2 \rangle < 0.1$. Upon cooling to 430 K a small jump to $\langle S_2 \rangle \approx 0.2$ is apparent indicating a transition to a more ordered phase has occurred at

this temperature. However, the time evolution of S_2 at 430 K (see Fig. 10b) does not display the large fluctuations in value characteristic of a NI transition. In addition, averaging S_2 over the entire trajectory results in $\langle S_2 \rangle < 0.15$, suggesting the system is effectively isotropic. At 420 K the time evolution of S_2 shows a dramatic increase to > 0.5 towards the end of the trajectory suggesting the onset of an ordered phase. In terms of the location of the simulated T_{NI} , these results indicate that 420 K $< T_{\mathrm{NI}} <$ 430 K which again is in good agreement with the experimental value of 421 K. These results are particularly encouraging and indicate that GAFF-LCFF is readily transferable to a variety of ODBP bent-core derivatives with chemically similar structures, with or without additional methyl substituents.

Conclusions

We have further improved and tested the GAFF-LCFF force field for use with bent-core liquid crystal molecules. Excellent clearing point predictions have been made for four bent-core oxadiazole derivative systems, using refined parameters for longer alkyl chains and ring-alkoxy junctions. The simulated estimates of T_{NI} were found to be within 10 K of experimental values for C5-Ph-ODBP-Ph-OC12, C4-Ph-ODBP-Ph-C7, C4O-Ph-ODBP and C4O-Ph-ODBP(trimethylated).

Simulations of the C5-Ph-ODBP-Ph-OC12 system indicate the presence of the experimentally observed dark conglomerate (DC) phase and a nematic to DC transition temperature within 15 K of the experimental value. This is the first time this has been observed in a molecular simulation.

Uniaxial orientational order parameters calculated for the C5-Ph-ODBP-Ph-OC12 system were compared with experimentally determined order parameters. In line with the experimental findings, these were found to be systematically lower when the bend angle was not accounted for. In addition, the average bend angle in the nematic phase of C5-Ph-ODBP-Ph-OC12 was found to be effectively temperature independent, supporting the assumption that a fixed bend angle may be used in obtaining order parameters from Raman data for ODBP bent-core systems.

Simulation system size effects were tested on the estimates of T_{NI} for the C4-Ph-ODBP-Ph-C7 and C5-Ph-ODBP-Ph-OC12 systems and were found to be small in comparison to errors in locating T_{NI}.

These results suggest that GAFF-LCFF is readily transferable to a range of liquid crystal mesogens based on the fragments and associated functional groups used in the parametrization process, including to a variety of oxadiazole bent-core derivatives with chemically similar structures, with or without additional methyl substituents. Further validation of GAFF-LCFF would ideally include the reproduction of additional experimental macroscopic properties besides phase transition temperatures. For example, phase diffusion coefficients, densities and viscosities are all important bulk phase properties, with direct relevance to applications. However, the experimental data for these are not currently available for the mesogens studied in this work.

Finally, ongoing work involves using this optimized force field (GAFF-LCFF) to understand the distinct, but often subtle, differences in molecular organization of the mesophases of this closely related group of bent-core liquid crystal molecules, as well as identifying a number of stucture-property relationships. It is anticipated that GAFF-LCFF will enhance the predictive capabilities of atomistic MD simulations, ultimately aiding in the design of novel LC materials.

Conflicts of interest

There are no conflicts of interest to declare.

Acknowledgements

The authors would like to thank Durham University for providing computer time on its high-performance computer system, Hamilton. The authors would like to thank Dr. Martin Walker for use of his pair distribution analysis codes and for valuable discussions.

References

1 R. Berardi, L. Muccioli and C. Zannoni, *ChemPhysChem*, 2004, **5**, 104–111.
2 G. Tiberio, L. Muccioli, R. Berardi and C. Zannoni, *ChemPhysChem*, 2009, **10**, 125–136.
3 F. Vita, T. Tauscher, F. Speetjens, E. T. Samulski, E. Scharrer and O. Francescangeli, *Chem. Mater.*, 2014, **26**, 4671–4674.
4 R. A. Reddy and C. Tschierske, *J. Mat. Chem.*, 2006, **16**, 907–961.
5 I. Cacelli and G. Prampolini, *J. Chem. Theory Comp.*, 2007, **3**, 1803–1817.
6 G. Prampolini, M. Campetella, N. De Mitri, P. R. Livotto and I. Cacelli, *J. Chem. Theory Comp.*, 2016, **12**, 5525–5540.
7 A. Pizzirusso, M. Savini, L. Muccioli and C. Zannoni, *J. Mat. Chem.*, 2011, **21**, 125–133.
8 I. Cacelli, C. F. Lami and G. Prampolini, *J. Comp. Chem.*, 2009, **30**, 366–378.
9 E. Kuprusevicius, R. Edge, H. Gopee, A. N. Cammidge, E. J. L. McInnes, M. R. Wilson and V. S. Oganesyan, *Chem.-Eur. J.*, 2010, **16**, 11558–11562.
10 F. Chami, M. R. Wilson and V. S. Oganesyan, *Soft Matter*, 2012, **8**, 6823–6833.
11 N. J. Boyd and M. R. Wilson, *Phys. Chem. Chem. Phys.*, 2015, **17**, 24851–24865.
12 C. Amovilli, I. Cacelli, S. Campanile and G. Prampolini, *J. Chem. Phys.*, 2002, **117**, 3003–3012.
13 M. Bizzarri, L. Cacelli, G. Prampolini and A. Tani, *J. Phys. Chem. A*, 2004, **108**, 10336–10341.
14 I. Cacelli, G. Prampolini and A. Tani, *J. Phys. Chem. B*, 2005, **109**, 3531–3538.
15 I. Cacelli and G. Prampolini, *J. Chem. Theory Comp.*, 2007, **3**, 1803–1817.
16 I. Cacelli, A. Cimoli, L. De Gaetani, G. Prampolini and A. Tani, *J. Chem. Theory Comp.*, 2009, **5**, 1865–1876.
17 L. De Gaetani and G. Prampolini, *Soft Matter*, 2009, **5**, 3517–3526.
18 X. Wei, J. B. Hooper and D. Bedrov, *Liq. Cryst.*, 2017, **44**, 332–347.
19 J. R. Schmidt, K. Yu and J. G. McDaniel, *Acc. Chem. Res.*, 2015,

48, 548–556.
20 J. Zhang, J. Su and H. Guo, *J. Phys. Chem. B*, 2011, **115**, 2214–2227.
21 Y. Olivier, L. Muccioli and C. Zannoni, *ChemPhysChem*, 2014, **15**, 1345–1355.
22 A. Pizzirusso, M. E. Di Pietro, G. De Luca, G. Celebre, M. Longeri, L. Muccioli and C. Zannoni, *ChemPhysChem*, 2014, **15**, 1356–1367.
23 A. Pizzirusso, M. B. Di Cicco, G. Tiberio, L. Muccioli, R. Berardi and C. Zannoni, *J. Phys. Chem. B*, 2012, **116**, 3760–3771.
24 M. F. Palermo, L. Muccioli and C. Zannoni, *Phys. Chem. Chem. Phys.*, 2015, **17**, 26149–26159.
25 H. Ramezani-Dakhel, M. Sadati, M. Rahimi, A. Ramirez-Hernandez, B. Roux and J. J. de Pablo, *J. Chem. Theory Comp.*, 2017, **13**, 237–244.
26 M. T. Sims, R. J. Mandle, J. W. Goodby and J. N. Moore, *Liq. Cryst.*, 2017, **0**, 1–17.
27 O. Francescangeli and E. T. Samulski, *Soft Matter*, 2010, **6**, 2413–2420.
28 O. Francescangeli, F. Vita, F. Fauth and E. T. Samulski, *Phys. Rev. Lett.*., 2011, **107**, 207801.
29 O. Francescangeli, F. Vita, C. Ferrero, T. Dingemans and E. T. Samulski, *Soft Matter*, 2011, **7**, 895–901.
30 S. Kaur, J. Addis, C. Greco, A. Ferrarini, V. Goertz, J. W. Goodby and H. F. Gleeson, *Phys. Rev. E*, 2012, **86**, 041703.
31 O. Francescangeli, F. Vita and E. T. Samulski, *Soft Matter*, 2014, **10**, 7685–7691.
32 F. Vita, I. F. Placentino, E. T. Samulski and O. Francescangeli, *Mol. Cryst. Liq. Cryst.*, 2013, **573**, 46–53.
33 F. Vita, T. Tauscher, F. Speetjens, C. Ferrero, E. T. Samulski, E. Scharrer and O. Francescangeli, *Mol. Cryst. Liq. Cryst.*, 2015, **611**, 171–179.
34 C. D. Southern, P. D. Brimicombe, S. D. Siemianowski, S. Jaradat, N. Roberts, V. Gortz, J. W. Goodby and H. F. Gleeson, *EPL-Europhys. Lett.*, 2008, **82**, 56001.
35 S. Pronk, S. Páll, R. Schulz, P. Larsson, P. Bjelkmar, R. Apostolov, M. R. Shirts, J. C. Smith, P. M. Kasson, D. van der Spoel *et al.*, *Bioinformatics*, 2013, **29**, 845–854.
36 A. W. S. da Silva and W. F. Vranken, *BMC research notes*, 2012, **5**, 367.
37 M. F. Palermo, A. Pizzirusso, L. Muccioli and C. Zannoni, *J. Chem. Phys.*, 2013, **138**, 204901.
38 M. R. Wilson and M. P. Allen, *Liq. Cryst.*, 1992, **12**, 157–176.
39 W. M. Haynes, *CRC Handbook of Chemistry and Physics, 92nd edition*, CRC press, 2011.
40 C. J. Dickson, L. Rosso, R. M. Betz, R. C. Walker and I. R. Gould, *Soft Matter*, 2012, **8**, 9617–9627.
41 G. Cinacchi and G. Prampolini, *J. Phys. Chem. A*, 2003, **107**, 5228–5232.
42 J. W. Emsley, G. DeLuca, G. Celebre and M. Longeri, *Liq. Cryst.*, 1996, **20**, 569–575.
43 S. Tsuzuki, H. Houjou, Y. Nagawa and K. Hiratani, *J. Phys. Chem. A*, 2000, **104**, 1332–1336.
44 S. A. R. Krishnan, W. Weissflog, G. Pelzl, S. Diele, H. Kresse, Z. Vakhovskaya and R. Friedemann, *Phys. Chem. Chem. Phys.*, 2006, **8**, 1170–1177.
45 J. Wang and T. Hou, *J. Chem. Theory Comp.*, 2011, **7**, 2151–2165.
46 S. Sui, K. Pluhackova and R. Bockmann, *J. Chem. Theory Comput.*, 2012, **8**, 1459–1470.
47 J. Pelaez and M. R. Wilson, *Phys. Rev. Lett.*., 2006, **97**, 267801.
48 H. F. Gleeson and P. D. Brimicombe, *Phys. Rev. Lett.*., 2011, **107**, 109801.
49 M. S. Park, B. J. Yoon, J. O. Park, S. Kumar and M. Srinivasarao, *Phys. Rev. Lett.*., 2011, **107**, 109802.
50 H. F. Gleeson, C. D. Southern, P. D. Brimicombe, J. W. Goodby and V. Gortz, *Liq. Cryst.*, 2010, **37**, PII 923874813.
51 D. Chen, Y. Q. Shen, C. H. Zhu, L. E. Hough, N. Gimeno, M. A. Glaser, J. E. Maclennan, M. B. Ros and N. A. Clark, *Soft Matter*, 2011, **7**, 1879–1883.
52 M. Alaasar, M. Prehm, M. Brautzsch and C. Tschierske, *Soft Matter*, 2014, **10**, 7285–7296.
53 M. Nagaraj, *Liq. Cryst.*, 2016, **43**, 2244–2253.
54 M. Nagaraj, K. Usami, Z. Zhang, V. GÃűrtz, J. Goodby and H. Gleeson, *Liq. Cryst.*, 2014, **41**, 800–811.
55 L. E. Hough, M. Spannuth, M. Nakata, D. A. Coleman, C. D. Jones, G. Dantlgraber, C. Tschierske, J. Watanabe, E. Korblova, D. M. Walba, J. E. Maclennan, M. A. Glaser and N. A. Clark, *Science*, 2009, **325**, 452–456.
56 M. Nagaraj, J. C. Jones, V. P. Panov, H. Liu, G. Portale, W. Bras and H. F. Gleeson, *Phys. Rev. E*, 2015, **91**, 042504.
57 M. Alaasar, M. Prehm, M. Brautzsch and C. Tschierske, *J. Mat. Chem. C*, 2014, **2**, 5487–5501.